Time-lapse analysis of CaMI.FRS CO₂ VSP data

Brendan J. Kolkman-Quinn[1], Donald C. Lawton[1,2], and Marie Macquet[2]

[1]CREWES, University of Calgary; [2]Carbon Management Canada

ABSTRACT

The Containment and Monitoring Institute Field Research Station (CaMI.FRS) operates a carbon sequestration experiment near Brooks, Alberta. By March 2021, 33 tonnes of CO_2 had been injected into a Basal Belly River Fm sandstone at 300m depth, as a simulation of a shallow leak from a CO_2 storage reservoir. Vertical Seismic Profiles (VSP) were collected between 2017 and 2021 to determine the detection threshold and monitor the plume of injected CO_2. These field data had high repeatability, with permanent borehole geophones and identical shot coordinates, with only surface conditions adding variability. A finite-difference VSP forward model was created to predict the 2D time-lapse response of the CO_2 plume and allow for testing of processing parameters with noiseless data. The 10Hz-150Hz field data required careful processing. A time-lapse compliant processing workflow was developed by paring down a standard VSP workflow, with the goal of avoiding unnecessary alterations to amplitude and phase. This simplified and minimized the cross-equalization between baseline and monitor amplitude spectra: Applying a pre-stack shaping-filter preserved most of the frequency content, at the cost of diminishing the amplitude of the CO_2 time-lapse anomaly. Alternatively, applying custom high-cut filters to the baseline and monitor shot gather pairs reduced the overall frequency content but preserved amplitude contrasts in the reservoir, yielding a higher-confidence result. The 2019-2017 time-lapse difference for a 15t of injection did not unequivocally detect the plume, showing a faint CO_2 anomaly amid background residuals of similar amplitude. The 2021-2017 results showed a higher-amplitude time-lapse anomaly similar to model's predictions. The normalized-root-mean-square (NRMS) difference between reflection amplitudes ranged from 10%-20% in the field data, above the noiseless model's NRMS of 8%-13%. The interpreted CO_2 plume had a 45m-51m lateral extent with an asymmetric distribution around the injection well, indicating greater permeation towards the south-west than to the north-east. A detection threshold between 15t and 33t of CO_2 in a 10% porosity reservoir has been confidently established. These findings will help inform Monitoring, Measurement and Verification (MMV) procedures at future CO_2 sequestration operations.

INTRODUCTION

The Containment and Monitoring Institute Field Research Station (CaMI.FRS) is a shallow CO_2 sequestration experiment near Brooks, AB, in western Canada. A primary research objective at CaMI.FRS is testing Measurement, Monitoring and Verification (MMV) capabilities for geological CO_2 sequestration. Multiple geophysical and geochemical monitoring technologies are employed at the FRS, including Time-lapse Vertical Seismic Profiles (VSP). Time-lapse VSPs have successfully been used for monitoring at other CO_2 sequestration operations (Bacci et al., 2017, Cheng et al., 2010), though a custom workflow was required for the CaMI.FRS data. The injection formation at the CaMI.FRS is the Basal Belly River Sandstone (BBRS), a brine-saturated reservoir of 10% porosity (Macquet and Lawton, 2017). The strong impedance contrast at the

interface between the BBRS and the overlying coal-and shale-bearing Foremost Fm produces a strong positive seismic reflection (Figure 1). The presence of gas-phase CO_2 in the reservoir at the FRS causes a decrease in the BBRS reflection amplitude, driven primarily by a decrease in P-wave velocity (Macquet and Lawton, 2019). This yields a time-lapse anomaly of negative amplitude.
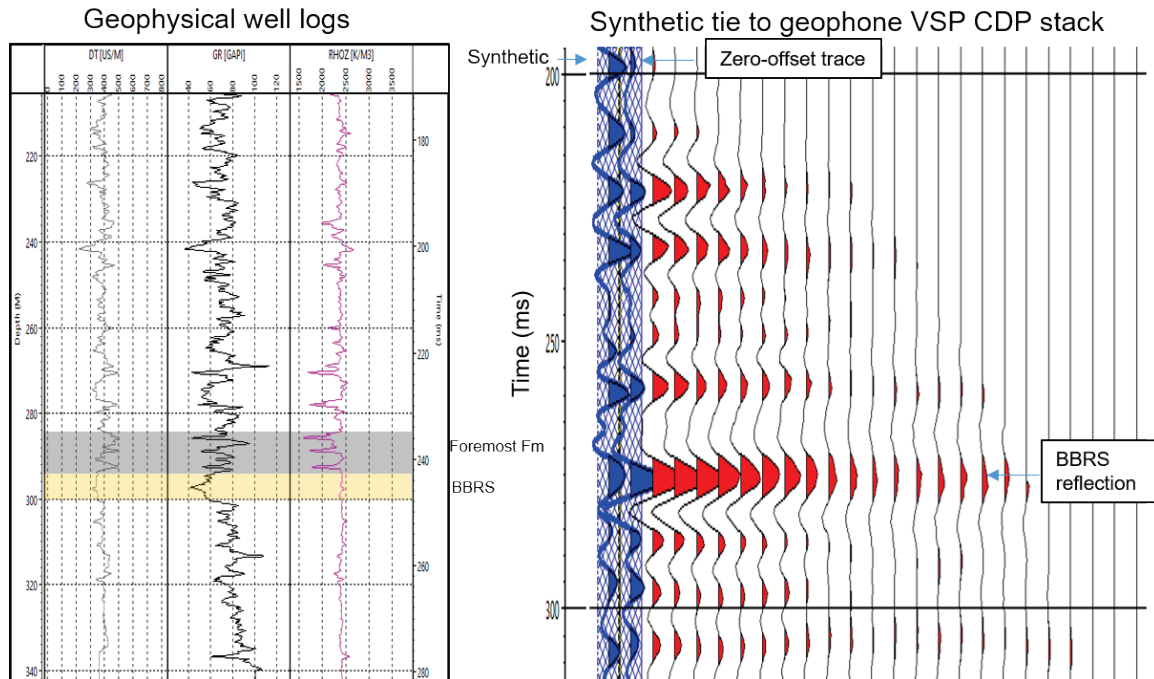

FIG. 1. Sonic, gamma ray, and density well logs with the Basal Belly River Sandstone (BBRS) highlighted in beige, and the coal-bearing Foremost Fm highlighted in grey. A synthetic trace is tied to a geophone VSP CDP stack on the right. The reflection at the interface between the Foremost Fm and BBRS produces a high amplitude, positive reflection.

Fluid substitution and finite difference modeling were performed to set expectations of the plume's effects on pre- and post-stack data. Using data from 2017, 2019, and 2021, the objectives of this work were to: Develop a reliable time-lapse compliant processing workflow for FRS VSP data, establish a detection threshold, and interpret the CO_2 plume.

DATASETS

Field data overview

Figure 2 shows a map view of the well and acquisition geometry at the FRS. VSPs data was collected in the geophysics observation well. The injection well (Inj) is offset from the geophysics well by approximately 20m to north-east, with a geochemical observation well (Obs 1) located a further 30m to the north-east. Monitoring surveys have been conducted periodically at the FRS since injection began in 2017. Figure 2 shows the map view of the walk-away VSP datasets with nearly identical acquisition parameters for time-lapse. The surveys are acquired using a vibroseis source with a sweep of 10Hz-150Hz. Lines 7, 13, & 15 are centered on the Obs 2 well and avoid the buildings and infrastructure on site, allowing for repeatable shot locations from survey to survey. Line 13 runs parallel to the three wells and was expected to be the first to show the CO_2 anomaly in a time-lapse

difference. While other VSP datasets from the FRS exist, including different walkway lines and Distributed Acoustic Sensing (DAS) data, the Line 13 geophone data was the most logical test-data for developing a standard time-lapse compliant workflow.
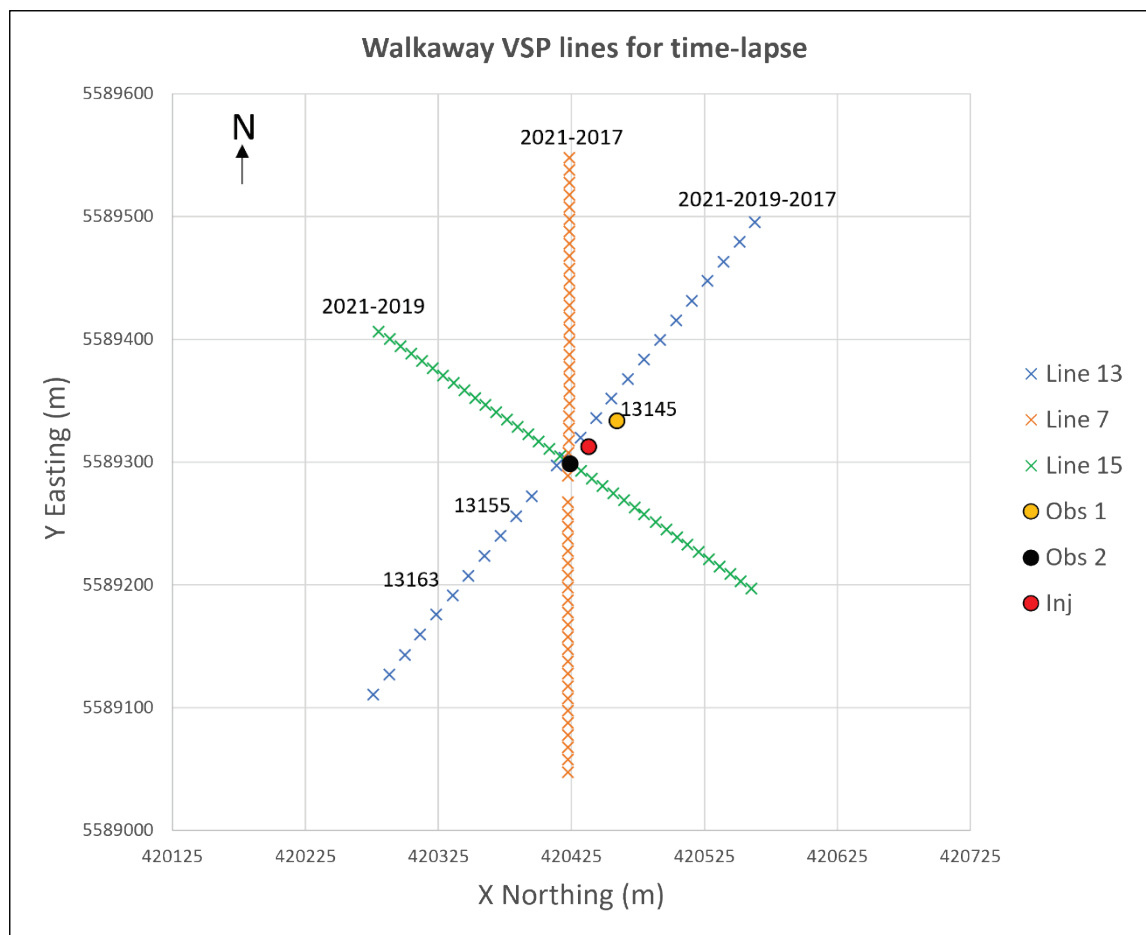

FIG. 2. Maps showing the positions of the injection well (red), geophysics well Obs 2 (black), geochemistry well Obs 1 (yellow). Walk-away VSP line 13 was used to design the time-lapse compliant processing workflow. Lines 7 and 15 will help delineate the CO_2 plume, once processed. The three shots marked 13145, 13155, 13163 are referred to throughout the report.

Observation well 2 (Obs 2) hosts 24 permanent, 3-component geophones spanning 190m to 305m depth, at 5m intervals. Shot spacing along line 13 was initially 20m in 2017, but reduced to 10m in subsequent surveys. To avoid introducing dissimilarity in the time-lapse, only the shot locations that existed for each pair of datasets were used. Available shot offsets span +/- 180m to +/- 250m depending on survey year. To avoid fold-imbalances in reflection CDP binning between baseline & monitor surveys, minor differences in shot locations (within +/- 2m) were treated as having identical source coordinates.

Injection amounts

Line 13 datasets from May 2017, August 2019, and both March 1st and March 25th, 2021 were processed. Table 1 shows the total mass of CO_2 injected between the baseline and monitor surveys. Although initial expectations were for a higher rate of injection (Macquet

and Lawton, 2017), the relatively small amounts of 15 tonnes and 33 tonnes of CO_2 at the time of the monitor surveys provided a valuable opportunity to establish a detection threshold for time-lapse VSPs in a shallow leak scenario. The limited plume extent also allowed for better calibration of the processing workflow, as individual datasets covered portions of the reservoir without CO_2 saturation, where time-lapse residuals should not occur.

Table 1. Total injected CO_2 between time-lapse surveys

Survey	Total injected CO2 (t)
2019 May	15
2021 March	33

VSP FORWARD MODELING

VSP model description

A VSP forward model was used to assist with trouble-shooting the time-lapse processing workflow and aid with interpretation of the field data. This finite-difference model used the CREWES Matlab® Toolbox and generated baseline and monitor shot gathers using acquisition geometry equivalent to the field data. The elastic properties of a 29t CO_2 plume were modeled based on previous fluid substitution and reservoir modeling work described by Macquet et al., (2019). This 29t modeled plume is comparable to the 33t total injection amount by March, 2021. The reservoir model is a well-log based 1D model, expanded into 2 dimensions. Figure 3 shows the CO_2 saturation and P-wave velocity reduction in a percent-difference display. The reservoir modeling predicts CO_2 saturation to be vertically consistent throughout the reservoir, with saturation decreasing horizontally out to a 25m radius. The modeled P-wave reduction caused by the presence of gaseous CO_2 is more vertically variable, due to mineralogy and porosity differences throughout the reservoir column. Due to the comparatively smaller effects of CO_2 saturation on density and S-wave velocity in the BBRS reservoir (Macquet et al., 2019), an acoustic model was deemed sufficient for the goals of this forward modeling exercise.
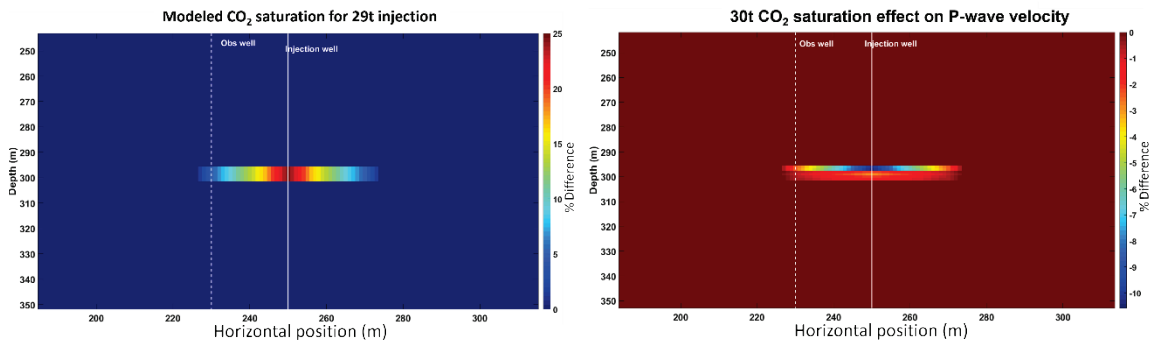

FIG. 3. Modeled CO_2 saturation and P-wave velocity reduction from 29t of CO_2. The CO_2 is contained in the 6m thick Basal Belly River Sandstone reservoir and the plume has a lateral extent of ~50m.

The model produced synthetic shot gathers in field-recorded time, using a ricker wavelet of 75Hz dominant frequency. This was adequately approximated the frequency content of the CaMI.FRS VSP data. No random noise was introduced to the data, as the goal was to test the effects of processing parameters on idealized data. The gathers were processed in a simplified version of a walk-away VSP processing workflow, with no need for static corrections and deconvolution. This yielded a synthetic VSP CDP stack and time-lapse difference, showing the synthetic CO_2 anomaly (figure 4).

As the observation well is offset by 20m from the injection well, the symmetric CO_2 plume model manifests as an asymmetric anomaly in the VSP CDP stack. This asymmetry is mainly caused by the offset-dependent fold distribution in the CDP bins. In field data, the asymmetry would be further enhanced by differential attenuation for farther offset CDPs. The synthetic anomaly is characterized by a reflectivity change and travel-time delay effect. The reduced acoustic impedance of the BBRS interval serves to decrease the amplitude of the strong positive reflection at the Foremost Fm – BBRS interface. A two-way travel-time delay of ~0.2ms is caused by the CO_2 plume, producing a lower amplitude 'tail' below the reflection anomaly. This small travel-time delay effect is expected to increase in prominence with greater vertical permeation of the CO_2 plume.
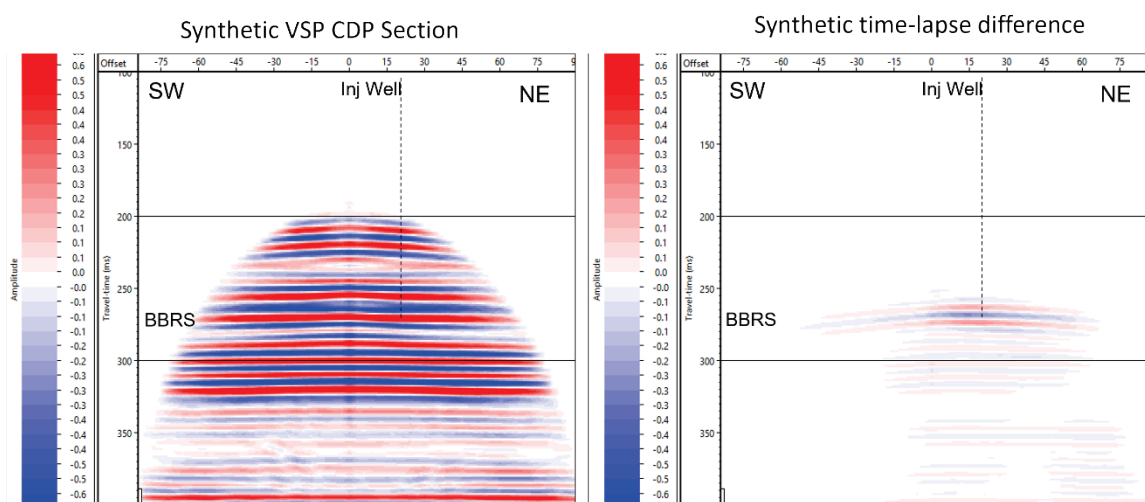

FIG. 4. Synthetic VSP CDP stack and time-lapse anomaly from 29t of CO_2, and reservoir interval indicated as BBRS. The reflection anomaly is in the form of a trough-peak succession with side-lobes, followed by a lower magnitude residual tail from travel-time delay through the CO_2 plume.

Synthetic time-lapse trouble-shooting

Previous time-lapse attempts with the CaMI.FRS VSP field data had yielded high amplitude coherent background residuals which threatened to obscure the time-lapse anomaly and impede its early detection (Kolkman-Quinn and Lawton, 2020). The VSP forward model allowed for testing the effects of minor residual static-errors, differences in frequency content in the field data, and determine the effects of a shaping filter on the CO_2 anomaly. Near-surface water-saturation and freeze-thaw effects introduced dissimilarity in the source signature between monitor and baseline surveys. Differences in near-surface statics, frequency content, and attenuation had been observed in the field data. Exacerbated by the high frequency (10Hz-150Hz) nature of these shallow VSP datasets, these near-

surface effects were expected to be the main source of unwanted, coherent residuals in the otherwise highly-repeatable time-lapse data. A cross-equalization step, using a shaping filter, was intended to mitigate these discrepancies (Al Mutlaq and Margrave, 2011). However, there was concern that the shaping filter would also diminish the amplitudes of the reservoir reflection and travel-time delay anomalies between baseline and monitor surveys. The VSP forward model allowed for testing the relative impacts of static errors, spectrum differences, and the shaping filter.
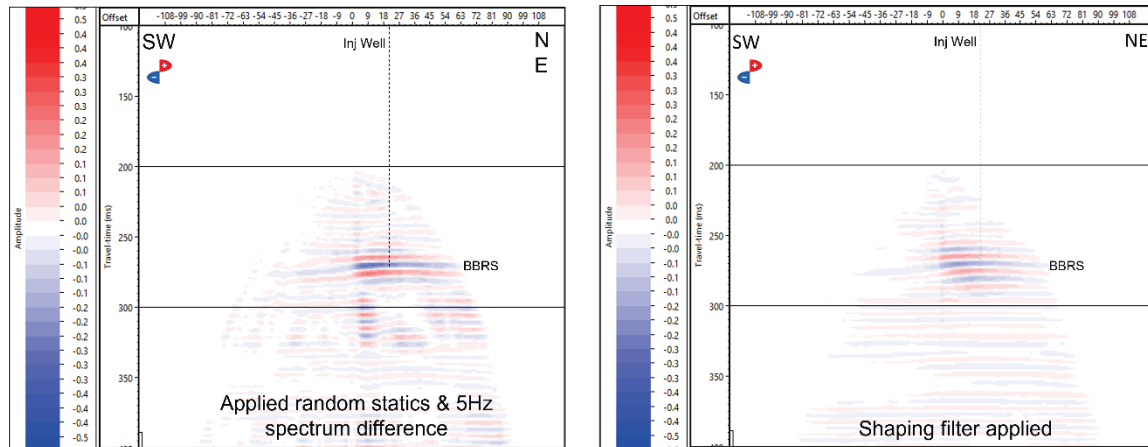

FIG. 5. Synthetic time-lapse anomaly with additional residuals caused by filtering 5Hz from the high monitor gathers' spectrum, and applying random shifts within +/-0.5ms to pre-stack gathers. The application of a pre-stack shaping filter eliminated most of the residuals but weakened the CO_2 anomaly.

Comparison of static-corrected First Break (FB) times (between baseline and monitor geophone field data) yielded average FB pick differences within +/-0.25ms. The first break times factor into normal move-out (NMO) corrections, two-way-time conversion, and VSP CDP mapping. Given the expected 0.2ms travel-time delay effect, the minor differences in FB pick times led to concerns of negatively affecting the time-lapse anomaly. Random static errors with various ranges, from +/- 0.1ms, 0.25ms, 0.5ms, 1ms, to 2ms, were applied to the synthetic monitor shot gathers to evaluate the impact on the time-lapse difference. It was determined that at +/- 0.5ms and greater, progressively worse coherent residuals manifested in the stacked synthetic time-lapse difference. At +/- 0.25ms, these static error residuals were not as damaging to the noiseless synthetic time lapse. These tests indicated that unresolved differences in frequency spectra were expected to be the more significant contributor of unwanted time-lapse residuals, though possibly compounded by static errors from inconsistent first break picks on particularly poorly-matched time-lapse shots.

Figure 5 shows the result of introducing a random static error of up to +/- 0.5ms to the synthetic shot gathers, coupled with a 5Hz frequency spectrum difference introduced by a bandpass filter. This artificial spectrum difference is a relatively small compared to the to field data. These alterations produced high amplitude, coherent residuals in the synthetic time-lapse difference, which increases the risk of misinterpretation of the anomaly. Applying a shaping filter eliminated much of the unwanted residuals (figure 5), but also diminished and the amplitude of the reflection anomaly. The travel-time delay anomaly was rendered indistinguishable from the background residuals. This highlighted the

importance of avoiding introducing unnecessary differences into the baseline and monitor during processing. This minimizes any negative effects that cross-equalization will have on the final time-lapse anomaly.

FIELD DATA PROCESSING

Eliminating processing-related error

Initial attempts at cross-equalization were informed by Cheng et al., 2010, involving shaping filters and root-mean-square amplitude normalization to balance amplitudes and frequency content. However, these initial attempts did not produce reliable, interpretable results with the CaMI.FRS data (Kolkman-Quinn and Lawton, 2020). To improve time-lapse compliance, the VSP processing workflow for FRS field data was further refined from those used by Gordon (2019) and Kolkman-Quinn and Lawton (2020), which had themselves been based on Hinds and Kuzmiski (1996) and the recommended workflows within Schlumberger's VISTA processing software.

The time-lapse compliant measures amounted to simplifying the existing workflows and removing as many amplitude scaling and filtering steps as possible. The objective was to avoid any processing steps that unnecessarily introduce differences between baseline and monitor surveys. Simplifying the workflow also made it easier to assess the downstream effects of each processing step in the final pre-stack gathers and stacked section. What follows is a summary of the removed processing steps:

- 3-component data rotation was removed. Only the vertical components of the geophones were used due to an increasing number of dead or sporadically malfunctioning horizontal components between 2017 and 2021. This eliminated error from both trace interpolation and hodogram analysis.

- Two mean-scaling steps (using first arrival amplitudes) were removed from the standard workflow. These steps were deemed redundant and error-prone compared to deterministic deconvolution and a simple time-power spherical divergence correction.

- Exponential gain, a final f-k filter, and a median filter were all removed from the VSP CDP stack process. These were in the standard workflow to account for absorption effects and clean up pre-stack gathers, but were deemed unnecessary.

- RMS amplitude normalization was removed from the baseline-monitor cross-equalization process. Amplitudes became directly comparable following the other changes, rendering this step unnecessary.

Following the removal of those processing steps, the testing of processing parameters and generation of time-lapse results became much more efficient and consistent. What follows is a description of the simplified VSP processing flow, with emphasis on the steps that were key to ensuring maximum similarity between baseline and monitor shot gathers.

Time-lapse compliant processing flow

First breaks and static corrections

First, raw data were phase rotated by -90 degrees prior to picking first breaks. In comparison with data from two different impulsive sources tested at the FRS, the vibe first arrivals superficially appeared phase-rotated by approximately -90 degrees (figure 6). This may be an artifact of the correlation of the vibe-sweep with a synthetic sweep. The vibe first arrivals in these datasets had previously been observed to contain high and low frequency artifacts, but as these are invariably removed by deterministic deconvolution, first-arrival waveform had not been a major source of concern. However, in comparing first break times after static corrections, it was determined that picking FBs on the phase-rotated data led to a closer match between baseline and monitor shot gather pairs. The first breaks were picked on a trough, equivalent to a compressional positive amplitude recorded by the upward-oriented vertical geophone component. In the un-rotated data, the first breaks in seemed to shift up or down with frequency content. Phase-rotating the data led to stable first breaks pick regardless of frequency content. These first break picks are used throughout the processing, crucially determining NMO corrections and two-way-travel time conversion. Any variability leads to artificial differences in the time-lapse comparison. This phase rotation had no impact on the final deconvolved reflection amplitudes. The phase rotation applies to both the upgoing and downgoing wavefields in the raw data. This rotation is then cancelled out during deconvolution of the downgoing from the upgoing wavefields.
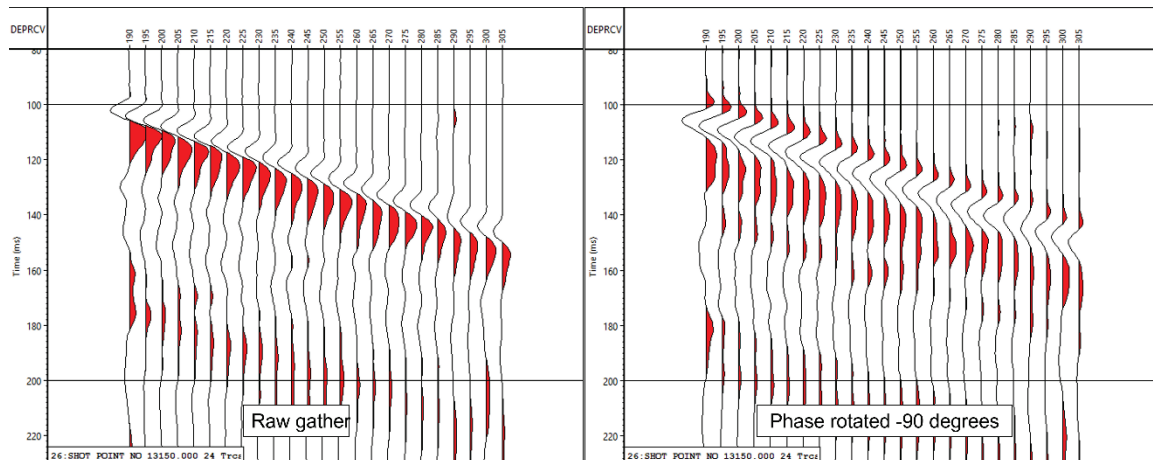

FIG. 6. Example of a raw shot gather (with interpolated dead traces) before and after a -90 degree phase rotation. The phase rotation led to a (superficially) zero-phase appearance. This resulted in stable 'trough' first break picks between baseline and monitor shot gathers despite differences in frequency content.

Four of the 24 vertical geophone components died after installation, and are missing in each of the datasets. These traces were interpolated prior to picking first breaks. Source-static corrections were applied to all datasets using the same velocity model for each dataset, in a process described by Lawton et al. (2019). This process adequately minimizes the differences in first break times between these geophone time-lapse datasets.

Wavefield separation

The data were then flattened to a 100ms datum and the downgoing wavefield was isolated using a 5-trace median filter (Gordon, 2019), applied to the raw data without mean-scaling of first arrival amplitudes. Median-filtering has reliably produced better final results than f-k filtering with these data. This median filter does not appear to significantly alter the individual first arrival amplitudes, and any minor effects on trace amplitudes were considered to be equivalent between time-lapse datasets. Due to the use of only the vertical geophone components, wavefield separation was accomplished by simply subtracting the downgoing wavefield from the raw data, and then applying an f-k filter to isolate and de-noise the upgoing P-wave reflections.

Deconvolution and scaling

Deterministic deconvolution was performed, using a window of -100ms to +200ms around the first break times. Trial and error testing with CaMI.FRS field data has determined that a long design window for the deconvolution operator works best to remove the artifact-ridden first arrivals of the correlated vibe-sweep. Less consistent results were obtained when using a short, 40ms-50ms window around the first arrivals. Extending the window -100ms before the first breaks helps capture the tails of the entire correlated waveform, and was also found to prevent the time-shift discrepancy between DAS and geophone data previously reported by Lawton et al. (2019).

It is important to note that no trace amplitude normalization was performed prior to deconvolution, unlike in standard workflows and in earlier processing attempts with these data (Gordon, 2019, Kolkman-Quinn and Lawton, 2020). Therefore, each trace's deconvolution operator contains amplitude and phase information on the cumulative effects of the source wavelet down to the time of the first arrival. These effects include filtering by the near surface (weather-related), spherical divergence, attenuation, and transmission loss. In a zero-offset shot gather, deconvolution effectively removes all of these effects from the reflection data in one step (figure 7).
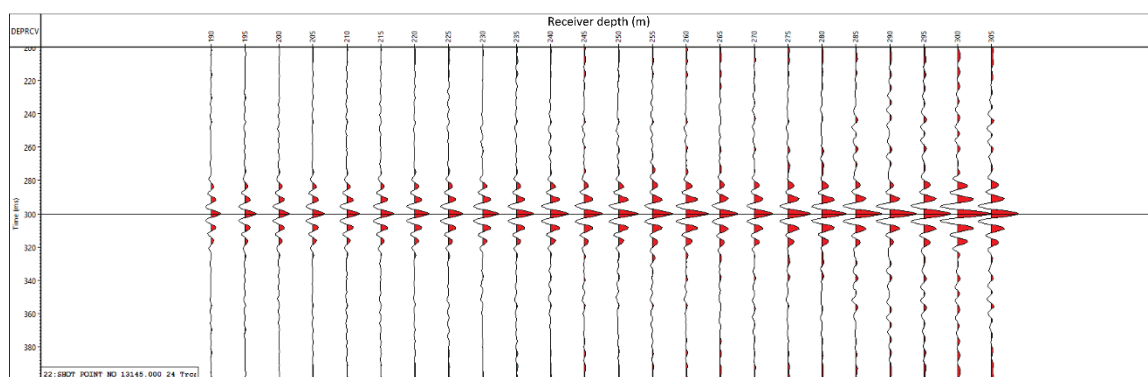

FIG. 7. Deconvolution operators from the downgoing direct arrivals. This example is from shot 13145, offset 50m NE from Obs 2. No scaling has been applied. The shallower receivers (left-side) have the highest amplitude and least attenuated direct arrivals. This leads to lower-amplitude deconvolution operators, with less high frequency scaling than the deeper operators (right-side).

Further attenuation and transmission loss effects remain in the reflection amplitudes as the reflected waves travel back up. Further spherical divergence was corrected for by multiplying flattened (-tt) reflection amplitudes by travel-time (T) to the power of one. This zero-offset assumption breaks down to some extent for farther offset shots, as the direct arrival does not share the same downgoing raypath as the reflected arrivals. However, in the FRS setting with a 300m deep reservoir, shot offsets to 250m, and similar ~2600m/s interval velocities above the reservoir, these assumptions seemed reasonable. The simplified scaling process led to the highest degree of similarity so-far-achieved between processed baseline and monitor shot gathers, reducing background residuals and eliminating need for further scaling during cross-equalization.
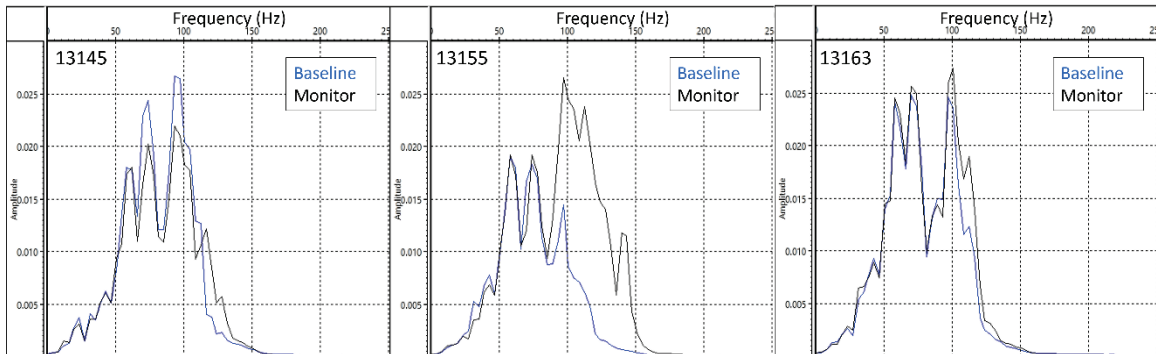

FIG. 8. Amplitude spectra of pre-stack gathers for shots 13145, 13155, and 13164 from 2021Mar1 (black) & 2017May (blue). Identical scales. Shot 13145 reflects off the CO_2 plume and shows a general decrease in amplitude from the strong BBRS reflection. 13155 and 13163 are SW of Obs 2 and do not reflect off the CO_2 plume. Deconvolved amplitudes match nearly exactly to ~80Hz, after which major (13155) and minor (13145, 13155) residual near-surface filtering effects remain.

In comparing deconvolved baseline and monitor reflection data, the low and medium frequency amplitudes match consistently between shot gathers, generally up to 75Hz-80Hz (figure 8). This indicates that time-lapse shot gather spectra have been properly scaled by deconvolution, and amplitudes are directly comparable without need of further scaling. Shot 13145 reflects off the CO_2 plume (figure 2) and has lower overall amplitude in the monitor data, indicating the CO_2 effect on the strong BBRS reflections. Some shots have nearly identical bandwidth (figure 8 – 13145, 13163), indicating similar near-surface filtering effects which have been mitigated by deconvolution. However, in other shot gathers there remain significant differences in bandwidth and high frequency attenuation (figure 8 – 13155). These differences cannot be entirely reversed by the deconvolution operator. These spectrum differences would cause high frequency residuals in the time-lapse difference and obscure the CO_2 plume anomaly. Pre-stack cross-equalization, discussed in a later section, was performed prior to VSP CDP stacking to minimize these residuals.

VSP CDP stack

Following wavefield separation, deconvolution, spherical divergence corrections, NMO corrections were applied to all datasets using the same velocity model. Data was then converted to two-way time equivalent (+tt), flattening reflected arrivals. At this stage, the processed pre-stack shot gathers were ready for cross-equalization prior to VSP CDP

mapping and stacking (discussed in the next section). Following cross-equalization, reflection data was mapped and sacked into 3m CDP bins, the smallest practical bin size for these geophone data.

CROSS-EQUALIZATION AND TIME-LAPSE RESULTS

Frequency content assessment

The geophone's limited coverage rendered post-stack shape-filtering impractical (Kolkman-Quinn and Lawton, 2020). Regardless, pre-stack cross-equalization was preferable. In the context of highly-repeatable CaMI.FRS VSP data, the cross-equalization step was intended to resolve the remaining baseline-monitor bandwidth and attenuation differences caused by weather-related near-surface filtering. Cross-equalizing the near-surface effects pre-stack was expected to result in greater similarity in the baseline and monitor data. Due to the high signal strength of the shallow geophone data (190m-305m) and the coherent appearance of the minimally-filtered reflection data, random noise and multiples were not a significant cause for concern.

Although field notes did not include weather and surface conditions observations, an appraisal of the relative frequency content of each survey shows a trend consistent with seasonal and monthly weather expectations. The baseline survey, acquired in May 2017 (2017May), is relatively low frequency. By comparison, the Aug 2019 survey (2019Aug) had generally broader frequency content and less attenuation. The March 2021 data (2021Mar1) was least attenuated, likely due to frozen ground conditions following prolonged cold weather in February 2021. Finally, the March 25th survey (2021Mar25) occurred after a particularly warm March with daytime highs consistently between 5^0C and 20^0C. This would have caused melting and poor transmission near the surface. This qualitative relationship is summarized in Table 2.

Table 2. Relative frequency content of baseline and monitor surveys

Survey	Relative Frequency content
2017May	Low
2019Aug	Medium
2021Mar1	High
2021Mar25	Low

Coincidentally, the May 2017 and March 25th, 2021 surveys yielded similar frequency content overall, but with shot to shot variability. This made it easier for a shaping filter to balance amplitude spectra between 2017May and 2021Mar25 datasets. Conversely, the 2021Mar1 survey had the broadest and least attenuated amplitude spectra, making it the easiest to apply high-cut filters to match the 2017May spectra. Both shaping filter and high-cut filter methods were applied, with the best results coming from 2021Mar1-2017May after high-cut filtering.

Normalized Root-Mean-Square difference

Normalized Root-Mean-Square (NRMS) was the principal metric used to quantitatively assess the similarity of the time-lapse results. The normalized root-mean-square difference (NRMS) between two seismic sections a_t and b_t is given by Equation 1:

$$NRMS = \frac{200 \, RMS(a_{t-b_t})}{RMS(a_t)+RMS(b_t)}.$$

(1)

Expressed as a percentage from 0% to 200%, lower NRMS values indicate high similarity. NRMS is sensitive to amplitude, phase differences, and random noise (Kragh and Christie, 2002).

Shaping filter method

Shaping filters minimize the difference between two datasets, and can be considered a least-squares solution to a matrix equation (Al Mutlaq and Margrave, 2011). Shaping filters were applied to the higher frequency monitor surveys in order to filter down towards the low frequency baseline. Based on trial and error testing, a 400ms design window and a 40ms operator length were used for the reflection data shaping filter design. The design window was chosen to avoid overfitting the shaping filter to the high amplitude BBRS reflection in the window. The shaped reflection data was not highly sensitive to the operator length parameter.
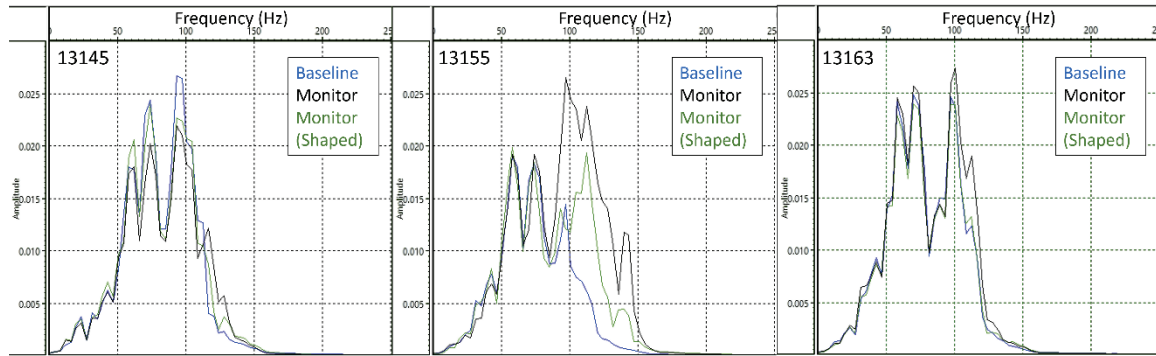

FIG. 9. Amplitude spectra of pre-stack gathers for shots 13145, 13155, and 13164 from 2021Mar1 (black) & 2017May (blue). Shape-filtered monitor data in green. In shot 13145, the shaping filter appears to negatively affect the interpreted reflection amplitude decrease from the CO_2 plume. The shaping filter adequately balances the very similar amplitudes in shot 13163, but fails to balance the extreme differences in shot 13155.

Figure 9 shows the effects of the shaping filter on the reflected amplitude spectra of shots 13145, 13155, 13163. In shot 13145 and 13163, the shaping filter equalized the already similar bandwidths. However, in 13145 it also raised the 50Hz-75Hz amplitudes closer to baseline. Assuming the original monitor data amplitudes were correct, this alteration would imply a weakening of the time-lapse anomaly. In shot 13155, the extreme spectrum differences were not eliminated by the shaping filter, leading to high frequency residuals. Shot 13163 began with a nearly identical spectrum, and the shaping filter successfully cross-equalized the minor differences. The results in figure 9 indicate that the shaping filter is not universally reliable for all shots, having the most difficulty equalizing very disparate frequency spectra.

A significant improvement in the time-lapse result was obtained by inspecting the pre-stack gathers for high levels of dissimilarity. Previous analysis had determined that the footprints of individual shots often manifested in the stacked VSP time-lapse result, causing coherent residuals (Kolkman-Quinn and Lawton, 2020). By calculating NRMS values for matching baseline-monitor shot pairs, particularly dissimilar shots could be identified for inspection (figure 10). After shape-filtering, these highly dissimilar shots typically caused the greatest amount of unwanted residuals. Figure 11 shows the effect of the shaping filter trying to reconcile very dissimilar and very similar shot gathers and the subsequent residuals. In the case of figure 11, the shaping filter is failing to raise up the frequency content of an anomalously low frequency monitor gather. However, anomalously high frequency monitor gathers also caused problems. In the 2021Mar25-2017 time-lapse, the following shots were removed due to large frequency content differences with the baseline: 13135 (low), 13147 (low), 13153 (low), 13161 (high). The removal of these dissimilar shot gathers significantly improved the stacked result by reducing coherent residuals.
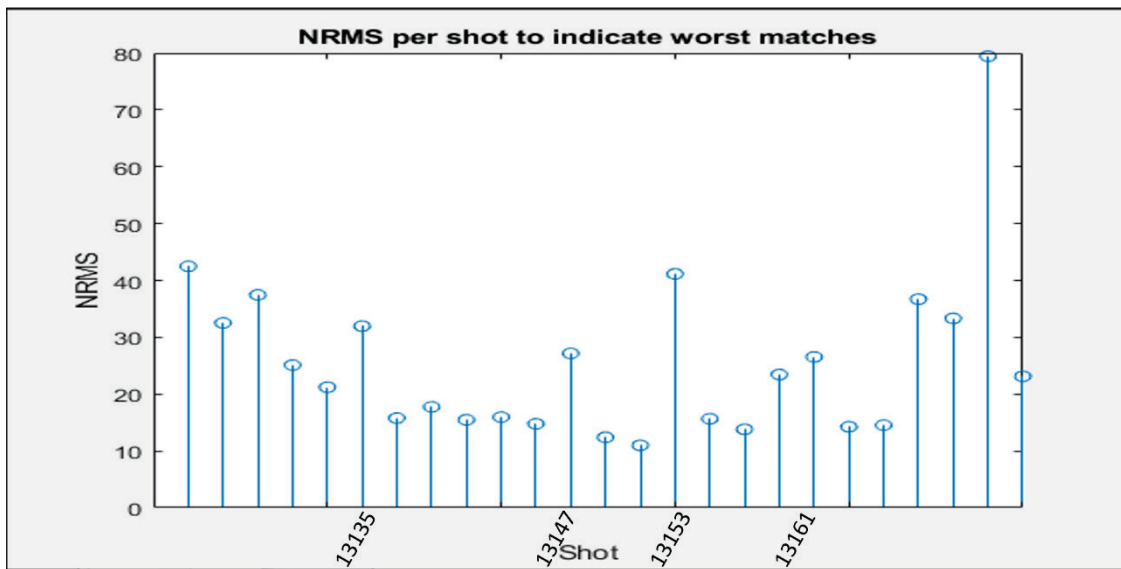

Fig. 10. NRMS values calculated for each baseline-monitor shot gather pair from the 2021Mar25 – 2017May time-lapse, prior to shape-filtering. The indicated shot numbers had anomalously high NRMS values above the trend, indicated particularly poorly matching shot gathers which remained unbalanced after shape-filtering. All shots were inspected to stacking but only these 4 were excluded.
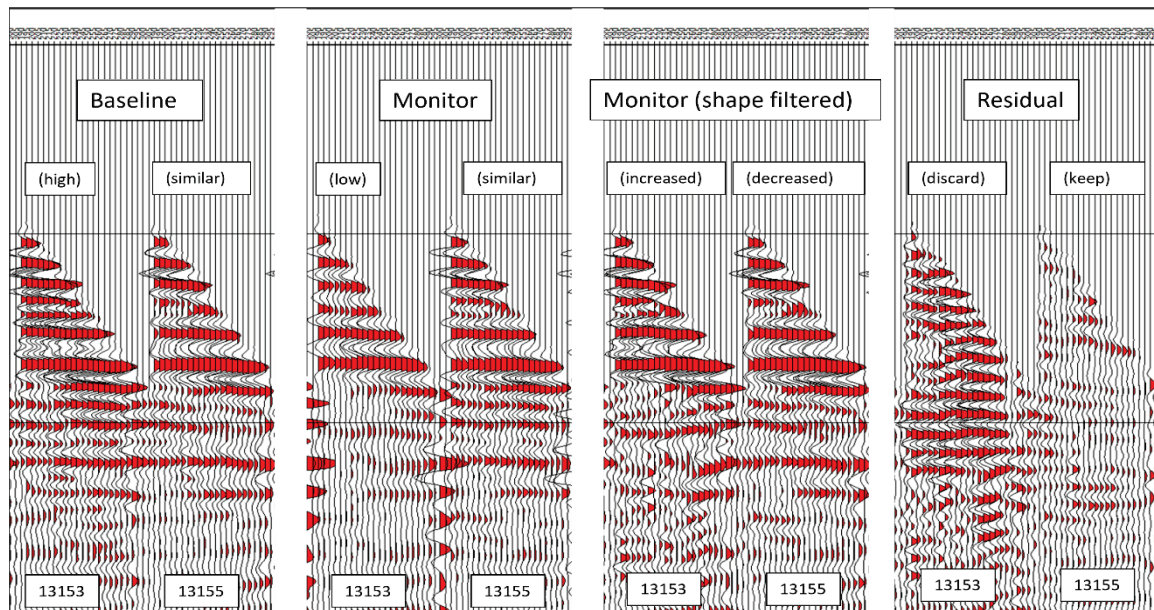
Fig. 11. Comparison of two shot gathers from 2017 May baseline and 2021 March 25th monitor data. After shaping-filtering, Shot 15 gathers remain much more dissimilar than Shot 16, causing significant residuals in the stacked time-lapse result.

After QCing and removing the worst-matching shots, the shape-filtered shot gathers underwent VSP CDP stacking and subtraction. The best result, from 2021Mar25-2017May, is shown in figure 12. An amplitude anomaly in the BBRS reservoir interval is apparent in figure 12b, extending from the injection well to the Obs 2 geophysics well. As shown in figures 5 & 9, it is likely that the CO_2 anomaly has been weakened by the shaping filter and does not stand out as clearly as it should from the background residuals. Below the anomaly, there exist relatively high amplitude residuals where travel-time delay residuals should occur. However, the travel-time delay effect was expected to be relatively weak prior to shape-filtering, and these residuals are more likely caused poor cross-equalization. Although the result in figure 12b likely does show some amplitude effects from the CO_2 plume, there was enough cause for doubt that a more direct cross-equalization was attempted using high-cut filters.
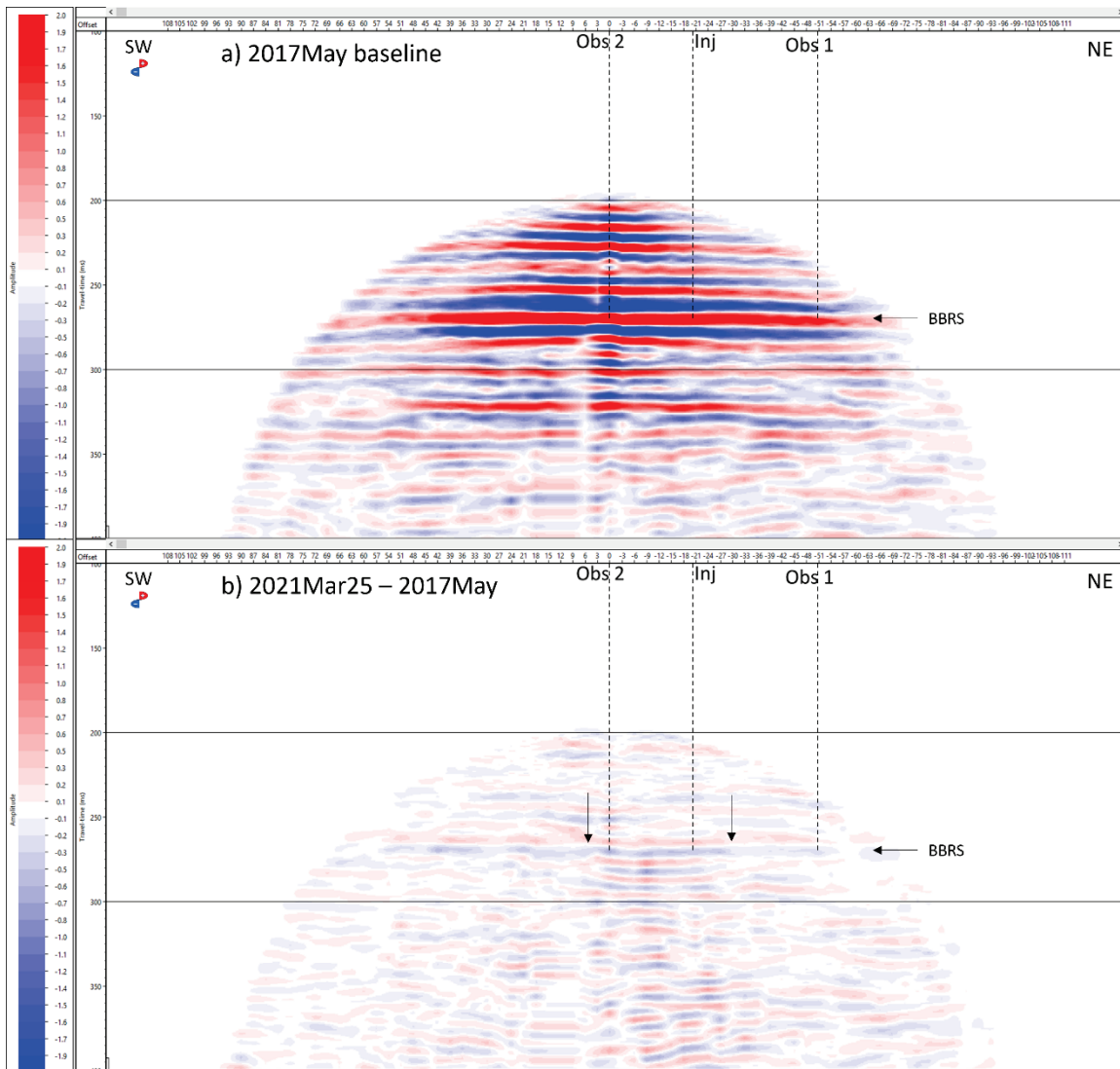
FIG. 12. VSP CDP stacked baseline and time-lapse difference for 2021Mar25-2017May datasets. The amplitude anomaly is most evident between the Obs 2 and Injection wells. BBRS interval and possible edges of the CO_2 plume are indicated by arrows. Unwanted residuals exist below the anomaly due to poor cross-equalization, casting doubt on the BBRS reflection anomaly.

High-cut filter method

The deleterious effects and inadequacies of the shaping filter (figure 5, figure 9 – 13145,13155) led to the idea of simply high-cut filtering the data down to a common bandwidth. The 2021Mar1 monitor survey was chosen to test this method, as none of its shot gathers had lower frequency content than the baseline 2017May, simplifying the process. Shot gathers were inspected individually and high cut frequencies were chosen. The goal was to trim the spectra at the point where they diverged significantly, leaving only the highest common frequency band where amplitudes appeared to match without obvious attenuation effects (figure 13). This laborious, brute-force process decreased the overall available frequency content, but avoided altering any relative amplitude differences in the remaining bandwidth (figure 13 – 13145). This was expected to preserve the CO_2 plume anomaly.
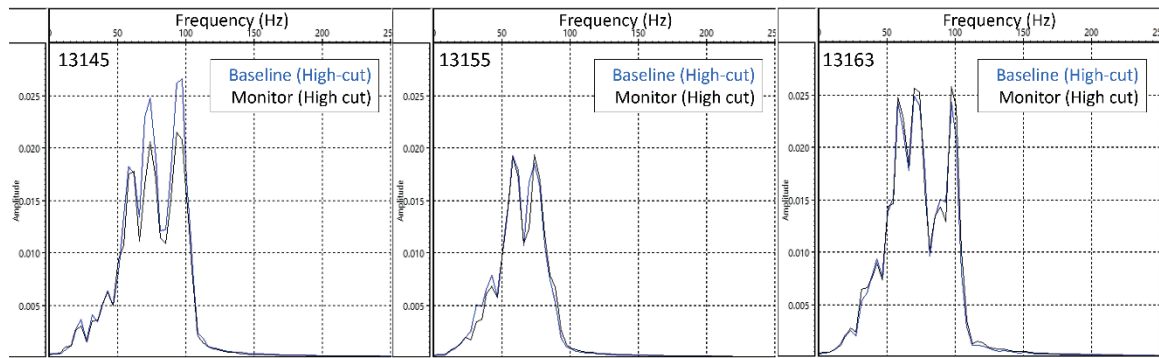
FIG. 13. Amplitude spectra of shots 13145, 13155, and 13163 after a custom bandpass filter of 5Hz-10Hz-XHz-YHz was applied to each shot. The frequencies X and Y were determined after visual inspection of each shot gather. The result was a common bandwidth with unaltered amplitudes for each baseline & monitor shot gather pair. Identical scales.

Some shots required no filtering at all, while others were grouped into categories with high pass – high cut frequencies of 50Hz-60Hz, 60Hz-70Hz, 75Hz-85Hz, 85Hz-95Hz, and 100Hz-110Hz. The stacked result (figure 14b) showed an unequivocal amplitude anomaly closely matching expectations from the synthetic (figure 4). The anomaly is a strong trough-peak succession with opposite side-lobe amplitudes. It appears localized at the BBRS interval though the travel-time delay anomaly may be visible below. Shot by shot inspection of VSP CDP mapped gathers appeared to show contributions to the amplitude anomaly from most of the north-east shots, increasing the confidence in this interpretation. The shot-by-shot inspection contributed to the conservative edge-of-plume picks of 15m SW & 33m NE indicated by arrows in figure 14b. However, the plume likely extends farther as lateral resolution is limited by the 3m binning and diminishing velocity anomaly of the CO_2 plume. An interpreted lateral plume extent of 45m-51m is in line with expectations from reservoir modeling (figure 3), except for its asymmetric spread towards the south-west. There was little spatial pattern to the filtering other than generally high levels of attenuation in the south-west far offsets of the 2017May data, visible in the unfiltered stack on the left hand side of figure 12. As a result, the frequency content and overall amplitude decreased erratically with shot offset rather than gradually, causing the wavy appearance of the anomaly in figure 14b.

With the successful 2021Mar1-2017May time-lapse result, the high-cut filtering process was repeated for the 2019Aug data which had the 2nd highest frequency content available. Several shots were lower frequency than in 2017, but most of the same filters could be used. This process was deemed impractical for the 2021Mar25 data, but may be attempted in the future. Figure 14a shows the 2019Aug-2017May time-lapse result. The two displays have identical horizontal scaling, but figure 14a has reduced coverage due to more limited shot offsets in 2019 (180m instead of 250m). There appears to be an anomaly standing out from the background residuals between the Injection well and Obs 2 in figure 14a. Arrows indicate the interpreted plume edge. However, the weaker anomaly would have been difficult to confidently identify without the 2021Mar1 interpretation of the 33t plume. Therefore, the 15t plume can be considered at or below the detection threshold.
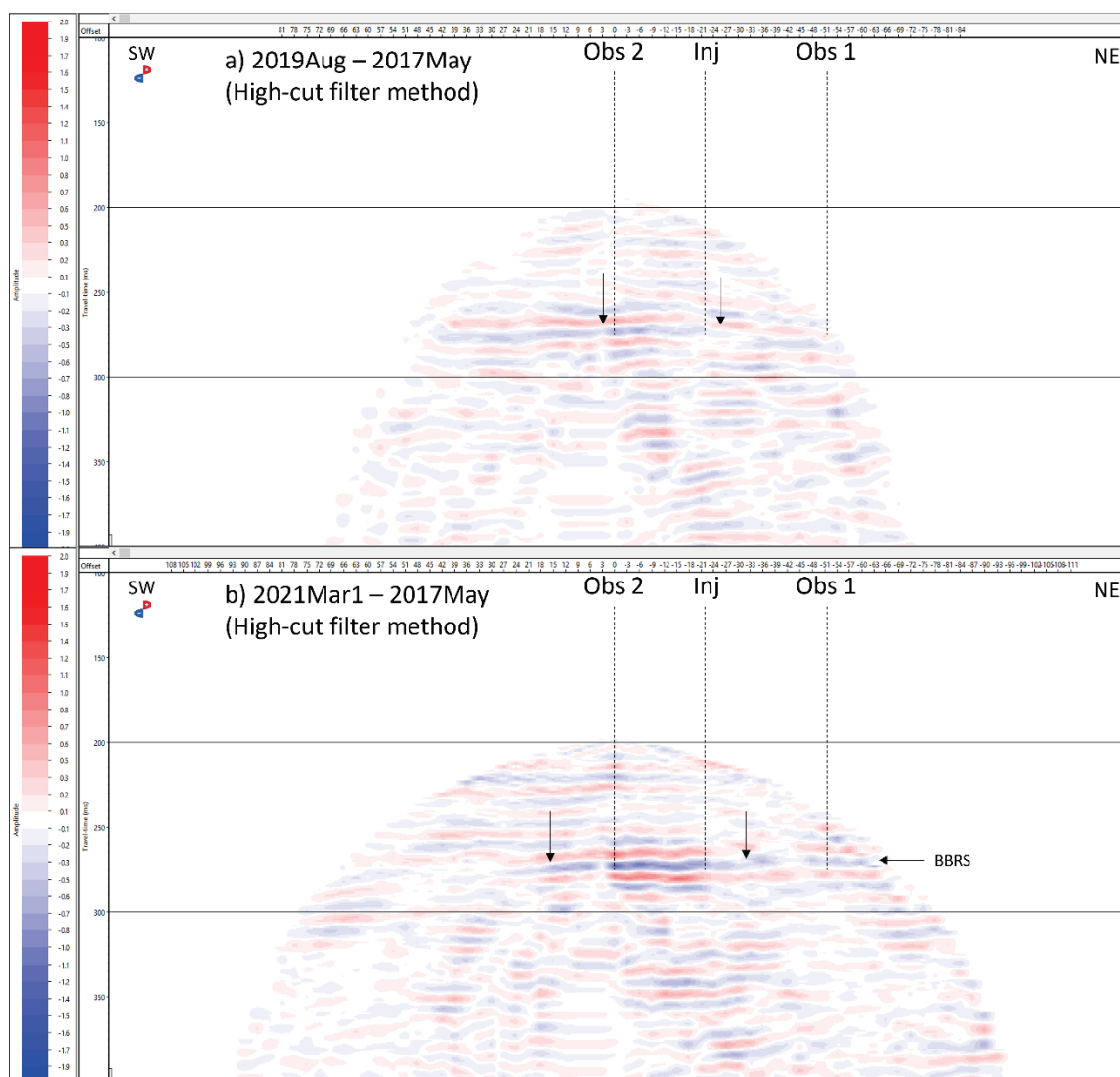
FIG. 14. VSP time-lapse results from 2019 and 2021Mar1 monitoring surveys using the high-cut filter method. The 33t time-lapse result in b) clearly shows the expected trough-peak CO_2 anomaly at the BBRS interval with side-lobe energy above and below. Two arrows indicate the conservatively-interpreted edge of the CO_2 anomaly. The 15t CO_2 plume may be present in panel a) but is not unequivocally above the detection threshold. Horizontal scale is identical; 2019Aug monitor survey had shot offsets limited to 180m rather than 250m.

DISCUSSION

In figure 14a, the 15t CO_2 plume was difficult to interpret with confidence as a stand-alone result. The possible reflection anomaly and travel-time delay at the injection well are relatively weak compared to the background residuals. In figure 14b, the 33t CO_2 plume causes a more pronounced time-lapse anomaly, clearly standing out from the background residuals. The shaping-filtered result in figure 12b was aided by having the highest similarity between raw baseline and monitor shot-pairs out of the available VSP datasets. However, the shaping filter appeared to diminish the magnitude of the reflection anomaly, both in pre-stack and post-stack data, while not satisfactorily mitigating background residuals.

Combined, the 2019 and 2021 time-lapse anomalies indicate the detection threshold for the plume was surpassed between 15t and 33t of injected CO_2. The 45m-51m lateral extent of the plume agrees with 50m expectation from reservoir modeling of a 29t plume (figure 3). The seismic anomaly extends beyond the Obs 2 well by 15m-18m but does not extend to the Obs 1 well which is at the limit of the geophone coverage. This is in agreement with the geochemistry observation well Obs 1 which had not detected the CO_2 plume by March, 2021, nor by November 2021 when this report was written.

Table 3 lists the associated NRMS values for the various time-lapse results discussed. The NRMS for the noiseless synthetic VSP time-lapse is 8% over a long window (150ms-400ms) and 12% over a shorter window (40ms) where the BBRS anomaly causes greater relative difference. The field data follow the opposite trend, with higher NRMS over the longer window than the short. This behaviour is due to background residuals. The high cut filtered 2021Mar1-2017May result has an improved 40ms NRMS of 15% due to the strong CO_2 anomaly, more in line with the model's NRMS. However it follows the same trend as the rest of the field data results. The longer window capturing the background residuals, and in combination with the BBRS anomaly, these cause a higher NRMS of 20%. This indicates that although the CO_2 anomaly has been preserved and is strong enough to stand out, the background residuals are not significantly weaker overall. In future time-lapse surveys, a trend of increasing NRMS in the 40ms window is expected as the plume grows laterally and vertically. However, with these data, NRMS would seem to be more useful as a diagnostic tool than as an interpretation tool.

Method	Time-lapse	Window	Field data NRMS	Modeled NRMS
Shaping filter	2019Aug-2017May	150ms-400ms	14%	n/a
		250ms-290ms	9%	n/a
Shaping filter	2021Mar25-2017May	150ms-400ms	15%	8%
		250ms-290ms	9%	13%
High-cut filter	2019Aug-2017May	150ms-400ms	15%	n/a
		250ms-290ms	10%	n/a
High-cut filter	2021Mar1-2017May	150ms-400ms	20%	8%
		250ms-290ms	15%	13%

Table 3. NRMS values from time-lapse results on monitoring line 13.

The successful 2021Mar1-2017May results raise two important points regarding future monitor survey acquisition and processing:

- The success of filtering down the 2021Mar1 data to the 2017 baseline highlights the value of frozen-condition winter surveys at CaMI.FRS, as the processing is simpler.

- As the CO_2 had evidently not progressed far beyond the Obs 2 well by 2019, some of the highly-attenuated south-western far-offset shots of 2017 can be

replaced with higher quality 2019 equivalents to form a hybrid baseline for Line 13.

The refined time-lapse compliant processing workflow can now be applied to monitoring lines 7 and 15 to better delineate the CO_2 plume in 3 dimensions. This workflow was designed for 1-component data and can be used for straight-fiber DAS data from Obs 2 and Obs 1.

CONCLUSION

A time-lapse VSP workflow was developed in order to detect the subtle effects of a small 33t CO_2 plume at 300m depth. With highly repeatable acquisition, the principal cause of dissimilarity between datasets was near-surface filtering resulting from weather related effects. The modified time-lapse processing workflow resulted in time-lapse differences with interpretable results which closely matched expectations from forward modeling. Coherent residuals were successfully mitigated, and CO_2 anomaly amplitudes were preserved by applying a high-cut filter to each processed shot gather, rather than a shaping filter. The simple, high-confidence geophone workflow and results can now serve as a basis for processing other VSP lines for geophone and DAS data from the CaMI.FRS. The detection of the 33t CO_2 plume with time-lapse walk-away VSP data establishes a detection threshold between 15t and 33t for this simulated shallow-leak field experiment in a 10% porosity sandstone. The detection of this known CO_2 plume has proven challenging until now, requiring a customized workflow and cautious processing even with highly repeatable, high frequency data. This indicates that detection of unknown leaks from a CO2 storage reservoir is not a trivial matter. Reservoir monitoring and early leak detection are key components of MMV requirements for geological CO_2 sequestration operations. For VSP monitoring of future storage projects, acquisition parameters should be designed not only for direct reservoir monitoring, but also for detection of possible leaks into shallower reservoirs.

ACKNOWLEDGEMENTS

REFERENCES

Al Mutlaq, M., and Margrave, G., 2011, Short note: Shaping / Matching filters: *CREWES Research Report*, **23**, 2, 11.

Bacci, V., O'Brien, S., Frank, J., and Anderson, M., 2017, Using a walk-away DAS time-lapse VSP for CO_2 plume monitoring at the Quest CCS project: CSEG Recorder, **42**, no. 3, 18-22

Cheng, A., Huang, L., and Rutledge, K., 2010, Time-lapse VSP data processing for monitoring CO_2 injection: The Leading Edge, **29**, 196-199

Gordon, A., 2019, Processing of DAS and geophone VSP data from the CaMI Field Research Station: M.Sc. Thesis, Univ. of Calgary.

Hinds, R.C., Anderson, N.L., and Kuzmiski, R.D., 1996, VSP Interpretive Processing: Theory and Practice: Society of Exploration Geophysics.

Kolkman-Quinn, B., and Lawton, D. C., 2020, Time-lapse VSP results from the CaMI Field Research Station: *CREWES Research Report*, **32**, 34, 14.

Kragh, E., and Christie, P., 2002, Seismic repeatability, normalized rms, and predictability: The Leading Edge, **21**, 640-647

Lawton, D. C., Gordon, A., Bidikhova, S., Hall, K. W., and Bertram, M. B., 2019, Update on DAS and geophone VSP surveys at the CaMI Field Research Station, Newell County, Alberta: *CREWES Research Report*, **31**, 39, 14.

Macquet, M., and Lawton, D., 2017, Reservoir simulations and feasibility study for seismic monitoring at CaMI.FRS: *CREWES Research Report*, **29**, 56.1-56.26

Macquet, M., and Lawton, D., Saeedfar, A., Osadetz, K., 2019, A feasibility study for detection thresholds of CO_2 at shallow depths at the CaMI Field Research Station, Newell County, Alberta, Canada: Petroleum Geoscience, **25**, 509-518